Geometry Controls Conformation of Graphene Sheets: Membranes, Ribbons, and Scrolls

Zhiping Xu[†] and Markus J. Buehler[†,‡,§,*]

[†]Laboratory for Atomistic and Molecular Mechanics (LAMM), Department of Civil and Environmental Engineering, , [‡]Center for Computational Engineering, and [§]Center for Materials Science and Engineering, Massachusetts Institute of Technology, 77 Massachusetts Avenue, Cambridge, Massachusetts 02139

ABSTRACT Graphene features a two-dimensional structure, where applications from electronic building blocks to reinforced composites are emerging, enabled through the utilization of its intriguing electrical, mechanical, and thermal properties. These properties are controlled by the structural makeup of graphene, which is known to display multiple morphologies that change under thermal fluctuations and variations of its geometry. However, as of now, a systematic understanding of the relationship between the conformation of graphene and its geometry remains unknown, preventing rational bottom-up design of materials, structures, and devices. Here, we present a conformational phase diagram for rectangular graphene sheets, defined by their geometry (size and aspect ratio), boundary conditions, and the environmental conditions such as supporting substrates and chemical modifications, as well as changes in temperature. We discover the occurrence of three major structural arrangements in membrane, ribbon, and scroll phases as the aspect ratio of the graphene nanoribbon increases. A theoretical and computational analysis of governing mechanisms for each conformation is provided.

KEYWORDS: graphene · two-dimensional materials · thermal fluctuation · phase diagram · self-folding

Two-dimensional thin film materials have received considerable interest recently due to their intriguing physical properties and viability for planar lithography and patterning processing. As an extreme example, the monatomic graphene membrane possesses unique features such as extraordinary electronic properties,[1] mechanical strength,[2] and ultrahigh thermal conductivity.[3] Graphene nanoribbons, the finite-width counterpart of crystalline graphene, are even more interesting as their edge shape and size control their electronic structure.[4] Experimental approaches using mechanical cleavage,[5] top-down lithography and cutting[6] and peeling,[7] chemical exfoliation,[8] and epitaxial growth[9] are now applied to fabricate graphene sheets with desired shape and size. The synthesized graphene sheets are subsequently transferred to various environments for specific applications, such as semiconductor/insulator substrates,[2] metal electrodes,[10] scaffolds,[11] or polymer matrices.[12] Previous atomic-scale microscopy and spectroscopy studies revealed a significant deviation of graphene conformations from a planar sheet in various environments, where ripples, kinks, and folds have been observed.[8,11,13] These characteristic "secondary structures" of graphene sheets have prominent effects on the resulting functional material properties and have thus received considerable attention.[14,15] For example, ripples with local curvatures create a charge inhomogeneity and a long-range scattering potential that changes the carrier mobility in graphene.[15] On the other hand, forming bilayered structures by depositing a graphene sheet on an existing one can provide flexible control of the band gap of graphene-based devices.[16]

As a result, from both theoretical and practical points of view, the question of what are the governing parameters that control the conformation of graphene sheet is crucial for applications of this material in devices and as functional materials. Can we predict the conformational phase diagram of graphene sheets, and how can we control conformational characteristics such as ripples and folds through specifying the geometry of graphene during fabrication or through environmental cues? Conformational fluctuations of low-dimensional materials at finite temperature are determined by their most thermally accessible phonon modes. In a graphene sheet, the out-of-plane bending mode (also known as the flexural phonon) has the lowest frequency and plays the dominating role. Moreover, the quadratic dispersion of this mode suggests a strong size-dependent phonon mode occupation and therefore results in a remarkable relationship between the geometry of graphene and its conformation.[17] To investigate this

*Address correspondence to mbuehler@mit.edu.

Received for review March 20, 2010 and accepted June 18, 2010.

Published online July 2, 2010. 10.1021/nn100575k

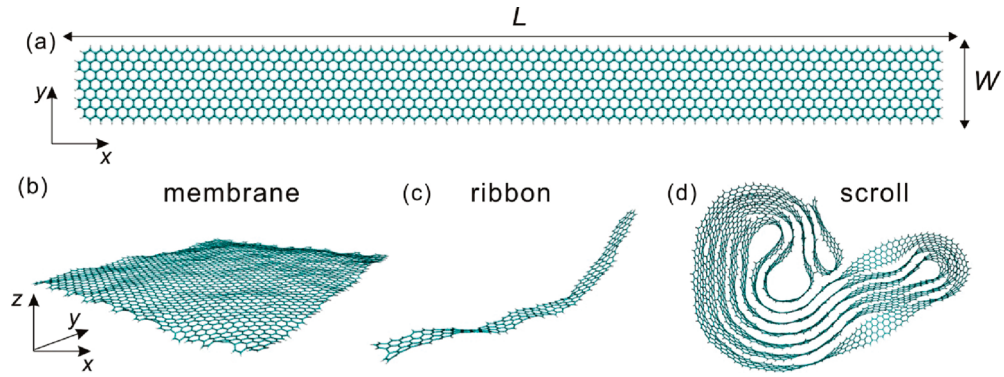

Figure 1. Structure and conformations of graphene sheets at room temperature. (a) Atomic structure of zigzag-edged graphene sheet with width *W*, length *L*, and aspect ratio $n = L/W$. The dangling σ bonds at open edges are terminated by hydrogen atoms. (b) Membrane conformation with intrinsic out-of-plane ripples observed in graphene sheet with an aspect ratio close to 1. (c) Ribbon conformation at $n = 11$. Bending and twisting along the contour length direction are observed. (d) Nanoscroll stabilized by van der Waals interaction between adjacent graphene layers at high aspect ratio ($n = 114$).

dependence, as well as to address the general questions raised above, here we perform a series of theoretical analyses and equilibrium molecular dynamics simulations to develop a systematic understanding of the phase diagram of graphene as a function of geometry.

The geometry of a rectangular graphene sheet is defined by its width *W* and length *L* ($L > W$), as shown in Figure 1a. The aspect ratio of the sheet is defined as $n = L/W$. The edge shape (along the length direction *x*) can be armchair, zigzag, or chiral—a mixture of armchair and zigzag edges that are thermodynamically unstable.[18] The width and edge shapes define the electronic properties of graphene nanoribbons.[4,19] On the other hand, since the graphene sheet with a hexagonal lattice is an isotropic elastic material, the edge shape does not change much of its structural and mechanical properties, especially in the elastic regime and with large radius of curvature in comparison with lattice constants. This is true for a thermal equilibrium state at room temperature, as considered in this work.[20] Therefore, for the finite-size structures where graphene sheet has open edges, we will focus on zigzag-edged graphene sheets along the lengthy direction (*x*) only. The open edges of graphene with dangling σ-orbitals on carbon atoms are not chemically stable in ambient environment, and we terminate them covalently with hydrogen atoms.

The basal plane of graphene is accessible for chemical modification such as epoxidation[21] and hydrogenation.[22] For basal plane hydrogenated graphene sheet, we randomly bind carbon atoms on the graphene sheet with isolated hydrogen atoms from both sides. Different hydrogenation densities (ratio between number of hydrogenated carbon atoms and all carbon atoms) $\rho_{H/C}$ ranging from 0.2 to 0.8 are investigated.

RESULTS AND DISCUSSION

Our simulation results reveal the existence of several distinct conformational phases of graphene sheets at room temperature, as summarized in Figure 1b−d. If the aspect ratio *n* is close to 1 (a quadratic shape), the conformation of graphene sheet resembles an elastic membrane with intrinsic ripples, as observed in experiemnts.[5,11] In this phase, the two dimensions (*x* and *y*) have comparable fluctuating amplitudes. As the aspect ratio increases, the morphology changes from that resembling a membrane to that of a quasi-one-dimensional ribbon. The ribbon phase has negligible deformation along its width (*y*) direction but remarkable bending and twisting along the length direction, resembling the structure of a flexible polymer chain. At even larger aspect ratios, the quasi-one-dimensional conformation self-folds into a graphene nanoscroll driven by interlayer van der Waals attractions between spatially adjacent parts of the nanoribbon. Multiple folds are formed in a cascade process for very long ribbons. The formation of these three phases distinctly depends on their geometric parameters: the size and aspect ratio. We now describe the mechanisms of the conformation formation and associated structural changes in detail for each of the three phases and use the information to develop a phase diagram.

Membrane Phase. Out-of-plane fluctuations with ripples are typical conformations of bulk thin films and membranes, which naturally arise from the coupling between in-plane stretching and out-of-plane bending modes. Graphene is the first two-dimensional crystal observed in experiments that was initially not expected to be thermodynamically stable. In the harmonic approximation for interatomic interactions in a two-dimensional crystal, it can be shown that the Fourier components of the correlation function for out-of-plane bending amplitude $h(x,y)$ with wave vector $\mathbf{q}$ is $\langle|h_{\mathbf{q}}|^2\rangle \sim T/(D\mathbf{q}^4)$.[23] The divergence of $\langle|h_{\mathbf{q}}|^2\rangle$ at small $\mathbf{q}$ with a large wavelength gives rise to the well-known paradox, which implies that a two-dimensional crystal will not exist. In graphene sheets, however, this paradox is resolved due to the anharmonic coupling between stretching and bending modes that suppress long wavelength fluctuations and stabilize the flat geom-

etry of graphene.[11,14] More specifically, graphene sheets buckle out of plane and form ripples instead of remaining as a flat crystal.

Membrane conformations of graphene sheets at low aspect ratios are sensitive to the boundary conditions, which can for example be characterized as with or without constraints on their open edges. For graphene sheets partially supported by scaffolds or electrodes, their edges are typically constrained through the adhesion with substrates or clamps at the bounday. The occurrence of thermal fluctuations with wavelength larger than their sizes is thus forbidden. In molecular dynamics simulations, these effects can be captured by the application of periodic boundary conditions to represent an infinite-size bulk material with a representative supercell. This, however, may have important implications on the observed conformations of graphene sheets. To explore this issue further, we perform simulations of square graphene sheet ($L = W$, $n = 1$) with L up to 50 nm. We observe a mean out-of-plane displacement amplitude of carbon atoms

$$\langle h \rangle = \sqrt{\sum_{i=1,N} m_i (h_i - h_{com})^2 / \sum_{i=1,N} m_i} \qquad (1)$$

on the order of 0.02 nm at room temperature. The amplitude has negligible changes up to $L = 50$ nm, reflecting the restraint on bending motion by the in-plane stretching elasticity. The averaging process shown in eq 1 is performed on all N atoms in simulation, m_i is the mass of the ith atom, and h_{com} is the center-of-mass position in the normal (z) direction of the whole graphene sheet.

Interestingly, the thermal fluctuation of graphene sheet features a one-dimensional wavy pattern $h(s) = C\sin(2\pi s/\lambda)$ instead of a two-dimensional checkerboard pattern $h(x,y) = C\sin(2\pi x/\lambda)\sin(2\pi y/\lambda)$, where s is the coordinate along fluctuation curve profile and C is the amplitude of out-of-plane fluctuation. The spatial extent of the one-dimensional ripple is $\lambda = 9$ nm (Figure 2a), in good agreement with previous experimental measurements[11] and Monte Carlo simulation results.[14] The patterns observed here resemble thin film buckles on a compliant elastomeric substrate, where the wave pattern is predicted to be energetically more favorable than the checkerboard pattern.[24] This argument can be made from an energetic point of view. The elastic bending energy E (the elastic energy due to bond stretching is neglected here as it is much smaller than the bending contribution) of a fluctuating membrane is given by

$$E = \int_A \frac{1}{2} D\kappa^2(x,y)\,dx\,dy \qquad (2)$$

where the integral is calculated over the whole membrane area A, κ is the mean curvature at position (x,y) and $D = 0.91$ eV is the bending rigidity (obtained directly from our simulation). As shown in eq 2, in comparison to the checkerboard pattern, the one-dimensional wavy pattern has a lower mean curvature at the same wavelength λ and amplitude C and is favored by lowering bending elastic energy. For a graphene sheet with this one-dimensional shape, the bending energy can be simplified as (with length L and width W)

$$E = \int_0^L \frac{1}{2} DW\kappa^2(s)\,ds \qquad (3)$$

where s is the coordinate along the bending profile, and $E = DLW\kappa_0^2/2$ (when the mean curvature is constant κ_0 along the profile). This model is valid as the deformation of graphene sheet can be represented by bending along the length direction and as confirmed

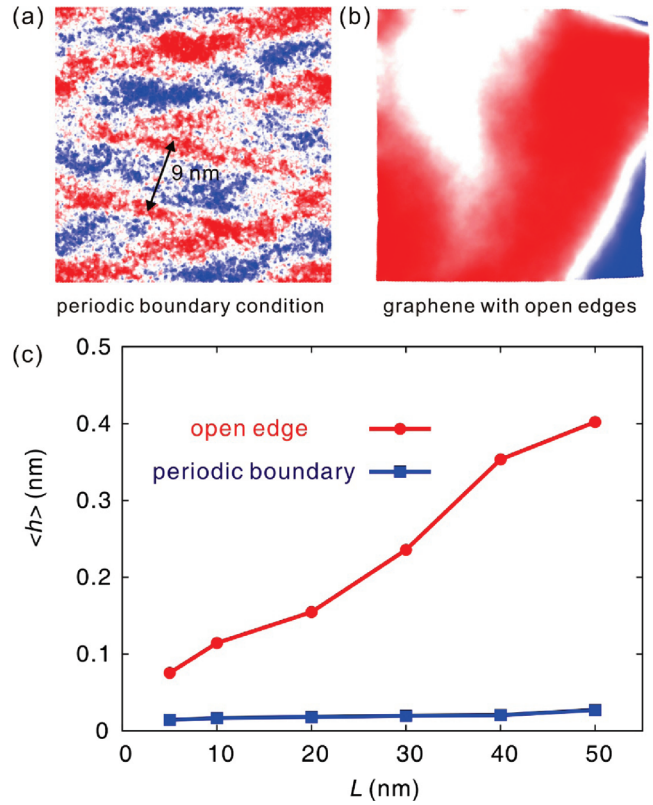

Figure 2. Out-of-plane displacement field and fluctuations in graphene sheets with different boundary conditions used to show that, in contrast to the short wavelength pattern under the periodic boundary condition, significant long wavelength fluctuation emerges in graphene sheets with open edges. The red and blue colors are positive and negative displacements along the out-of-plane z direction, respectively. (a) One-dimensional wavy pattern under periodic boundary conditions, where the deformation is bound by the bending and stretching elastic energy as a finite curvature is created. The displacement field has a typical length scale at 9 nm. (b) Diverging displacement field under open-edge boundary condition. The fluctuations have a much larger amplitude but small local curvatures. The red and blue colors represent positive and negative displacement in the normal direction of the original flat sheet. (c) Averaged out-of-plane displacement amplitude $\langle h \rangle$ (see eq 1) of both graphene sheets with periodic boundary condition (a) and open edges (b). The results demonstrate that fluctuations are limited under periodic boundary condition (on the order of 0.02 nm) and diverge as the size increases when the long wavelength fluctuation mode becomes accessible under open-edge boundary conditions.

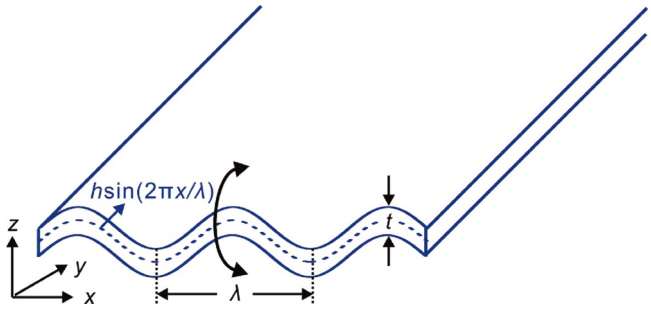

Figure 3. Change of the second moment of bending I_y (eq 4) due to a one-dimensional out-of-plane deformation h sin(2πx/λ).

from our simulations the contribution from bending contributes most to the elastic energy.

On the other hand, for free-standing graphene sheets or those suspended in solution, the restraints at the boundary are removed and open edges are free. Therefore, bending modes with large wavelength are allowed, preferred, and dominate their fluctuation pattern. To illustrate this effect directly, we further perform simulations for free-standing graphene sheets of finite size. It is noticeable that in these structures, carbon atoms at open edges are not stable due to the dangling σ bonds. Significant residual stress will arise at the edges and drive static edge wrapping.[25] We thus terminated them with hydrogen atoms to mimic experimental conditions. Equilibrium molecular dynamics simulation results show that out-of-plane thermal fluctuations are significantly magnified in comparison with boundary constrained ones (see Figure 2 for a comparison between the two cases). In addition to the short wavelength fluctuation at edges (Figure 1b), the out-of-plane displacement pattern extends to the whole sheet and has a larger amplitude.

The out-of-plane fluctuation of graphene sheet is highly restricted when the periodic boundary condition is applied as the long wavelength phonons are forbidden. Instead, the fluctuating amplitude of open-edge sheet continues to rise as the size of graphene sheet increases (Figure 2c). For larger-scale graphene sheets whose size exceeds our computational abilities, the radius of gyration of an elastic membrane is expected to diverge with size as $R_g \sim (\ln L)^{1/2}$.[26]

To investigate the effects of substrate and chemical modifications, we also perform simulations for bilayer and basal plane hydrogenated graphene sheets. Our results show that thermal fluctuation is greatly reduced due to the enhancement of bending rigidity $D = YI$ in both cases for sheets at small aspect ratios, where Y is the Young's modulus and I is the second moment of inertia of the sheet. In bilayer graphene where thickness t is doubled, $I = Wt^3/12$ is enhanced by a factor of 8. In the hydrogenated graphene sheet, neighboring carbon−hydrogen bonds repel each other and thus

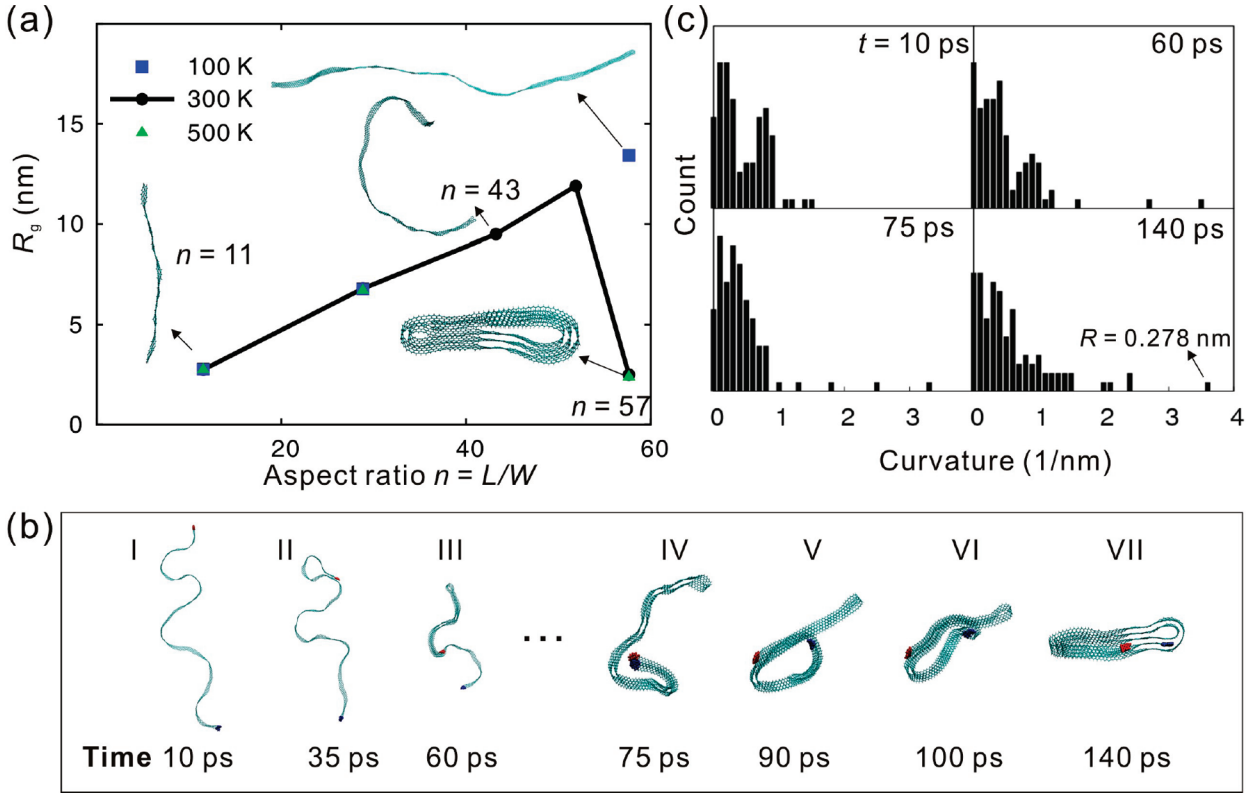

Figure 4. Dependence of graphene sheet conformation on aspect ratio (with fixed width W = 1 nm). (a) As the aspect ratio n increases, graphene nanoribbon changes from planar membrane, worm-like nanoribbons, to nanoscrolls. The radius of gyration is proportional to the length of ribbon before self-folding occurs. At low temperature (T = 100 K), the thermally induced bending curvature of graphene nanoribbon is much smaller than the T = 300 and 500 K, and the self-folding is prohibited. (b) Evolution of local curvatures for the graphene nanoribbon with n = 57. (c) Snapshots from the simulation to show the folding dynamics of the formation of nanoscrolls.

avoid local bending. The planar conformation of graphene sheet can also be stabilized by a cohesive substrate such as SiC, SiO_2, and metals which are widely used in deposition[18] or epitaxial growth[9] of graphene. Strongly binding substrates with mismatching lattice constants can even result in static and periodic buckling patterns of graphene sheet.[9]

Ribbon Phase. Our results for small aspect ratio graphene sheets with periodic and open boundary condition simulations both show a one-dimensional wavy fluctuation pattern instead of two-dimensional ripples. This is because, as we will see, when an out-of-plane bending deformation along one direction is formed, the resistance to bending along another direction will be significantly enhanced. Considering the graphene sheet as an isotropic elastic membrane and $D = YI$, out-of-plane fluctuation $h(x,y)$ of graphene sheet modifies I significantly, especially as the fluctuating amplitude $\langle h \rangle$ is comparable to the thickness of graphene sheet, which is very small ($t = 0.066$ nm)[27] in an elastic thin-shell model.

As illustrated in Figure 3, when the membrane is bent along one dimension (x for example), with a sinusoidal function $h(2\pi x/\lambda)$, the membrane is much more difficult to bend on the other dimension simultaneously. The bending moment along the other dimension (y)

$$I_y = \int z^2 \mathrm{d}A = \frac{\lambda t^3}{12} + \frac{\lambda h^2 t}{2} = I_{0y} + \Delta I_y \qquad (4)$$

where I_{0y} is the moment of inertia for the planar sheet. The relative correction taking into account a periodic modulation with wavelength λ and amplitude $2h$ ($y = h \sin 2\pi x/\lambda$) is $f = \Delta I_y/I_{0y} = 6(h/t)^2$ is the enhancement factor. The modulation of out-of-plane fluctuation in the x direction of amplitude 0.1 nm can result in a prominent enhancement factor $f = 13.77$ and can thus effectively prohibit fluctuations in the out-of-plane direction y. In fact, this effect has been widely applied in macroscale engineering, such as using corrugated steel in construction applications.

As the aspect ratio n reaches values greater than 1, the conformation of graphene sheet changes from that resembling a membrane to a nanoribbon. The fluctuation along the length direction further stabilizes its quasi-one-dimensional conformation according to eq 4. As a result, the nanoribbon assumes polymer-like chain conformations (as shown in Figure 1c and Figure 4). Thermal fluctuations along the width direction are negligible; however, a coexistence between local bending and twisting is observed along the contour length of nanoribbons. To quantify this conformational transition from membrane to quasi-one-dimensional chain from our simulation data, we calculate the radius of gyration R_g from

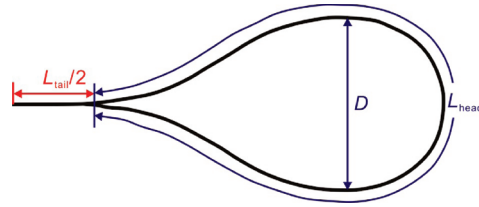

Figure 5. Geometry of the self-folding of a graphene nanoribbon for energetic analysis in eqs 7−9 (into a "tennis-racket" shape).

$$R_g^2 = \sum_{i=1,N} \sum_{\alpha} m_i (r_{i,\alpha} - r_{com,\alpha})^2 / \sum_{i=1,N} m_i \qquad (5)$$

that measures the compactness and characterizes the conformational anisotropy. In eq 5, $r_i = (r_{i,x}, r_{i,y}, r_{i,z})$ is the spatial position of atoms i, and $\alpha = x, y, z$. The results show that as we increase the aspect ratio n from 1 to higher values, the radius of gyration R_g for nanoribbon increases with linear dependence (Figure 4a), demonstrating the one-dimensional behavior of the ribbon. After a critical value $n_{cr} = 50$, one part of graphene becomes able to contact others within the same nanoribbon and the nanoribbon self-folds into a nanoscroll, giving rise to yet another structural phase.

Scroll Phase. As in the polymer chains, the persistence length of graphene nanoribbons

$$l_p = DW/k_B T \qquad (6)$$

characterizes the length scale above which entropic factors will dominate (and orientational order is kept only below this length scale). For graphene nanoribbons with width $W = 1$ nm, $l_p = 35$ nm. Graphene ribbons with length L beyond this value tend to form wedges, loops, or globular structures, as driven by thermal fluctuation and the loss of orientational order. This theoretical estimate of the persistence length is consistent with our simulation results, as shown in Figure 4a. The critical aspect ratio $n_{cr} = l_p/W = D/k_B T$ has an inversely linear dependence on the temperature T. When $T = 100$ K, the graphene nanoribbon maintains its one-dimensional morphology. The self-folding is not accessible at $n = 57$, where it folds at $T = 300$ and 500 K.

As shown in Figure 4b, the self-folding starts from a large amplitude bending motion from one end of the nanoribbon. When two parts of the nanoribbon start to contact after an initial correlation time, surface tension drives the contacted segments to slide with respect to each other rather rapidly, creating more contacts. The sliding speed is on the order of 100 m/s, which is close to the value of the atomic thermal motion speed. A sliding speed of the same order is also observed in double-walled carbon nanotubes[28] and diffusing benzene molecule on graphite, as observed in experiments, thus validating the findings from our simulations.[29] At the final stage of folding dynamics, multiple folds form in the graphene ribbon in a series of cascades. The whole collapse process finishes in 140 ps, and the system

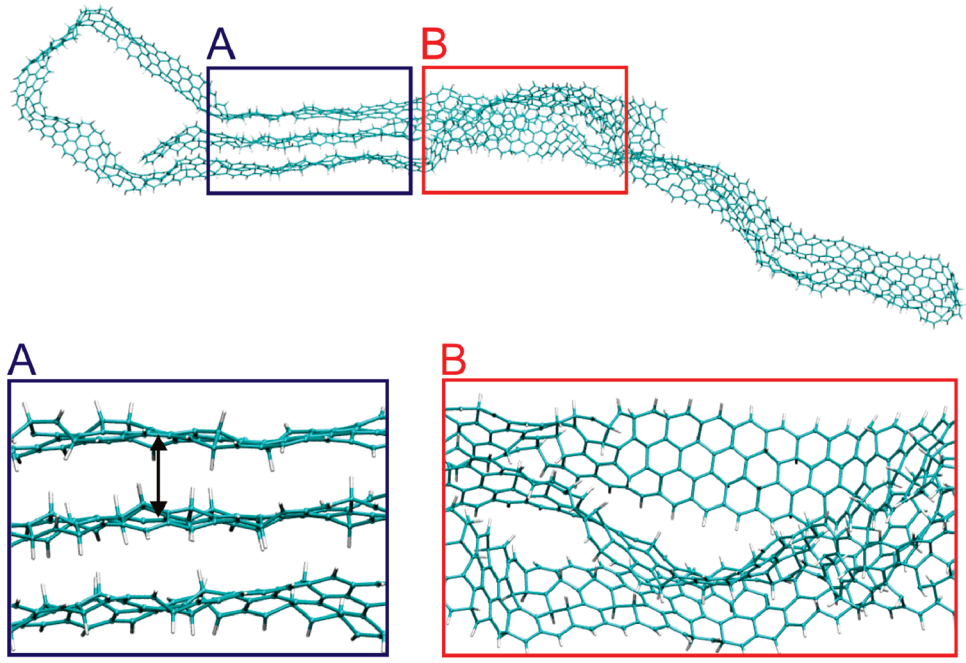

Figure 6. Self-folding of a hydrogenated graphene nanoribbon (density $\rho_{H/C} = 0.3$). The C−H groups and corrugated basal plane prohibit interlayer sliding and leave partially folded structures that are locally stable. The two regions shown in greater detail show one segment with planar stacking order and a twisted segment that is locked by the large resistance to interlayer sliding motion due to carbon−hydrogen bonds, respectively.

eventually reaches a thermodynamically stable folding conformation with a dumbbell shape. The heads of the dumbbell have a characteristic maximum radius of curvature. To calculate the curvature along the graphene nanoribbon, the coordinates are first averaged along the width. The chain conformation obtained is then coarsened into segments with length of two unit cells (0.49 nm) to filter out local fluctuations. A cubic spline function is used to interpolate the chain and evaluate the local curvature. The simulation result (Figure 4c) shows discrete values, reflecting a regular folding pattern. The maximum radius of curvature is 0.278 nm, which is controlled by the balance between elastic and surface energy in graphene sheets.

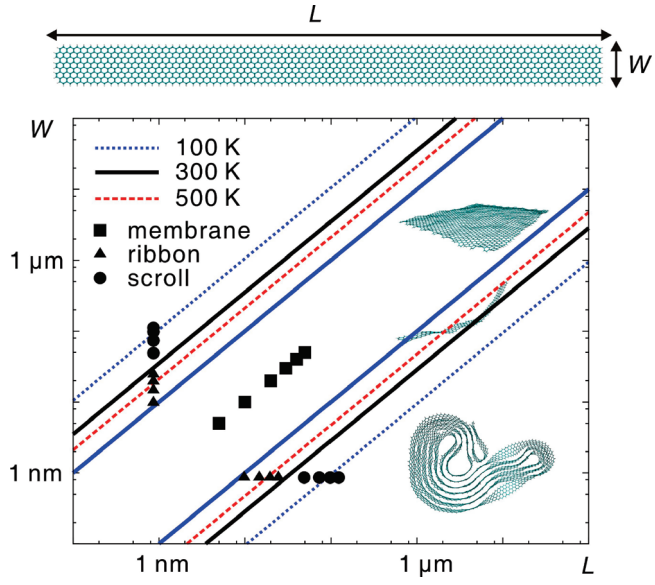

Figure 7. Conformational phase diagram of graphene sheet at room temperature ($T = 300$ K) as a function of the length L and width W (solid lines), as well as the change of behavior under variations of temperature. When the length and width are similar ($n < 10$), the graphene sheet keeps a conformation of planar membrane. As n increases, ribbon phase appears and it self-folds into scrolls (scroll phase) as the length exceeds the persistence length. We plot the geometry of systems in our study as discrete points and mark the equilibrium phase (filled square for membrane, triangle for ribbon, and circle for scroll phase). The theoretical predictions are consistent with the molecular dynamics simulation results. The variations of the boundary between ribbon and scroll phase according to eq 6 are also plotted as the temperature changes to $T = 100$ K (dotted lines) and 500 K (dash lines).

Although the kinetic access to self-folding is controlled by the persistence length l_p, the final shape of the nanoscrolls is determined by energetic driving forces. Specifically, the critical length of folds can be evaluated through *elastica* theory. On the basis of eq 3, *elastica* theory predicts the elastic energy of bendable graphene to be

$$U = \int_0^{L/2} \left[\frac{D}{2}\left(\frac{\partial\theta}{\partial s}\right)^2 + \varsigma\cos\theta\right] W ds \qquad (7)$$

where ς is the Lagrange multiplier used in the variational principle method, which has the dimension of a force and represents the force required to keep the contact between graphene sheets.

With variation principle, the Euler equation can be finally deduced as $dq/ds = 2b(1-k^2\sin(\theta/2))^{1/2}/k$ and the bending energy can be expressed through the elliptic function $U = \beta DW\int d\theta(1 - k^2\sin^2(\theta/2))^{1/2}/k = 2\beta DW/kE(\theta/2,k)$, where $k = 1.1695$ is the elliptic modulus as determined from the corresponding geometrical con-

straint. A numerical solution of this function shows that the "tennis racket head" energy is $A(D/L)W$ where $A = 18.3331$.[30,31] The result is very close to that of a circular ring with the same contour length $2\pi^2 DW/L = 19.7392DW/L$. The driven force is van der Waals interaction between adjacent graphene layers. Therefore, the energy of the a nanoscroll can be written as (Figure 5)

$$E = E_{bending} + E_{vdW} = ADW/L_{head} + \gamma WL_{tail} \quad (8)$$

where $E_{bending}$ and E_{vdW} are energy terms arising from bending of graphene sheet and interlayer cohesion, L_{head} and L_{tail} are the contour length under bending and interlayer cohesion respectively, and $L_t = L_{head} + L_{tail}$ is the total length of graphene nanoribbon that is constant. The balance between bending energy and intersheet cohesion energy gives a critical length for folding of graphene nanoribbons as

$$l_c = L_{head} + L_{tail} = L_{head} + AD/(-L_{head}\gamma) \quad (9)$$

so energetically speaking, the onset of self-folding in graphene sheet requires l to be large than $l_c = 8.61$ nm, which is less than the persistence length l_p, and thus l_p governs transition between ribbon phase to the scroll.

We also investigate the dynamics of a graphene sheet that has been hydrogenated on its basal plane. As shown in Figure 6, we find that the graphene ribbons fold into scrolls eventually. However, the sliding process is prohibited and replaced by a number of discrete clamping processes. The ordered region of hydrogenated graphene ribbons also presents a planar structure with interlayer distance of 0.4 nm instead of 0.32 nm in bare graphene ribbons.

Phase Diagram. From the discussion above and a combination of eqs 2 and 3, we can obtain a phase diagram for free-standing graphene sheets. When the dimensions of length L and width W are close to unity, the graphene sheet keeps a conformation of planar membrane ($n < 10$). As n increases, ribbon phase appears and it can self-fold into the scroll phase as the length exceeds persistence length ($l > l_p$, that is, $n = L/W > D/k_BT$). The interface between ribbon and scroll phases can be modified by the temperature T as the persistence length l_p (eq 6) depends linearly on $1/T$. As depicted in Figure 7, our simulation results at room temperature correspond well with this predicted diagram. Moreover, the boundary conditions and chemical absorptions and the presence of supporting substrates as discussed above can further modify this phase diagram. For example, adhesion from supporting substrates or due to a multilayer structure of graphite sheets will result in enhanced bending rigidity and persistence length and thus shift the length scale for transition between membrane, ribbons, and scrolls at a given temperature. It should also be noted that the predictions put forth in this diagram may break down when the width or length of graphene sheet approach the size of benzene molecules, where dihedral deformation becomes significant.

CONCLUSION

In summary, we have presented a systematic analysis that demonstrated that the conformation of graphene sheets is controlled by its geometry (size and aspect ratio) and environmental conditions such as surface modifications and substrate. The rich science of graphene sheet morphology discussed here links concepts from thin film or membrane theory at small aspect ratio n (patterns for thermal fluctuation or mechanical instabilities) and polymer physics (persistence length) at large n. The extreme geometric confinement present in nanoribbon structures, together with unique intraribbon van der Waals interaction, gives rise to intriguing physical phenomena, which may lay the foundation for future applications and device design. Moreover, the concepts explored here could also be applied to other low-dimensional materials such as boron nitride monolayers, polymeric membranes, and lipid bilayers.

With the availability of advanced fabrication and lithography techniques for large-scale graphene applications, the phase diagram provided here (Figure 7) could enable the directed design of graphene-based materials and devices. For example, our results demonstrate that low aspect ratio graphene nanoribbons are better for electronic applications because self-folding is avoided. Further, nanoscrolls can be assembled from high aspect ratio structures, which may be useful for a variety of interesting applications including oscillators[32,33] and hydrogen storage. Also, preprocessed one-dimensional structural modulations[34,35] of graphene sheets can reduce thermal fluctuations by preserving phonon coherence. The remarkable effects from substrate and chemical treatment imply many additional engineering possibilities that could be explored in future works.

METHODS

Molecular Dynamics Simulations. We perform molecular dynamics simulation using the LAMMPS package.[36] The adaptive intermolecular reactive empirical bond-order (AIREBO) potential function[37] is employed to calculate interaction between carbon and hydrogen atoms, which includes both covalent bonding (stretching, bending, torsion, and others) expressed in terms of bond orders, as well as van der Waals interactions between atoms at a larger distance. These two parts of the energy contribution in this potential yield bending rigidity D and surface energy γ of graphene as 0.91 eV and -9.05 meV/Å^2. The bending rigidity is calculated by comparing potential energy E_{CNT} of an armchair carbon nanotube of various diameters d with graphene sheet E_g (*i.e.*, $E_{CNT} - E_g = 2\pi DW/d$). The energy difference between bilayer and monolayer graphene $(E_{bilayer} - 2E_{monolayer})/2S$ gives surface energy γ, where S is the contact area between two graphene sheets.

We apply periodic boundary conditions for infinitely large graphene sheets, where conformational fluctuations with wavelengths exceeding the periodic box length are omitted. We perform canonical molecular dynamics simulation with constant temperature $T = 300$ K to investigate the conformation of graphene sheet. The atomic structure is initially optimized using a conjugated gradient method. The Nosé−Hoover algorithm with a time constant of 0.1 ps is used for temperature control in subsequent constant temperature (*NVT*) simulation. For systems with periodic boundary conditions, a pressure control is applied to release the in-plane residue stress using the Berendsen algorithm. For all dynamical simulations, a time step of 0.5 fs is used. The total simulation time is 7 ns, including a 5 ns initial setup phase during which conformation fluctuations converges, and 2 ns production simulation to analyze the data in equilibrium, that is, the conformational fluctuations of graphene sheets.

Acknowledgment. This work was supported by DARPA and the MIT Energy Initiative (MITEI).

REFERENCES AND NOTES

1. Geim, A. K.; Novoselov, K. S. The Rise of Graphene. *Nat. Mater.* **2007**, *6*, 183–191.
2. Lee, C.; Wei, X.; Kysar, J. W.; Hone, J. Measurement of the Elastic Properties and Intrinsic Strength of Monolayer Graphene. *Science* **2008**, *321*, 385–388.
3. Balandin, A. A.; Ghosh, S.; Bao, W.; Calizo, I.; Teweldebrhan, D.; Miao, F.; Lau, C. N. Superior Thermal Conductivity of Single-Layer Graphene. *Nano Lett.* **2008**, *8*, 902–907.
4. Son, Y. W.; Cohen, M. L.; Louie, S. G. Energy Gaps in Graphene Nanoribbons. *Phys. Rev. Lett.* **2006**, *97*, 216803–216804.
5. Meyer, J. C.; Geim, A. K.; Katsnelson, M. I.; Novoselov, K. S.; Obergfell, D.; Roth, S.; Girit, C.; Zettl, A. On the Roughness of Single- and Bi-Layer Graphene Membranes. *Solid State Commun.* **2007**, *143*, 101–109.
6. Ci, L.; Xu, Z.; Wang, L.; Gao, W.; Ding, F.; Kelly, K.; Yakobson, B.; Ajayan, P. Controlled Nanocutting of Graphene. *Nano Res.* **2008**, *1*, 116–122.
7. Sen, D.; Novoselov, K. S.; Reis, P. M.; Buehler, M. J. Tearing Graphene Sheets from Adhesive Substrates Produces Tapered Nanoribbons. *Small* **2010**, *6*, 1108–1116.
8. Li, X.; Wang, X.; Zhang, L.; Lee, S.; Dai, H. Chemically Derived, Ultrasmooth Graphene Nanoribbon Semiconductors. *Science* **2008**, *319*, 1229–1232.
9. Sutter, P. W.; Flege, J.-I.; Sutter, E. A. Epitaxial Graphene on Ruthenium. *Nat. Mater.* **2008**, *7*, 406–411.
10. Chen, C.; Rosenblatt, S.; Bolotin, K. I.; Kalb, W.; Kim, P.; Kymissis, I.; Stormer, H. L.; Heinz, T. F.; Hone, J. Performance of Monolayer Graphene Nanomechanical Resonators with Electrical Readout. *Nat. Nanotechnol.* **2009**, *4*, 861–867.
11. Meyer, J. C.; Geim, A. K.; Katsnelson, M. I.; Novoselov, K. S.; Booth, T. J.; Roth, S. The Structure of Suspended Graphene Sheets. *Nature* **2007**, *446*, 60–63.
12. Stankovich, S.; Dikin, D. A.; Dommett, G. H. B.; Kohlhaas, K. M.; Zimney, E. J.; Stach, E. A.; Piner, R. D.; Nguyen, S. T.; Ruoff, R. S. Graphene-Based Composite Materials. *Nature* **2006**, *442*, 282–286.
13. Li, Q.; Li, Z.; Chen, M.; Fang, Y. Real-Time Study of Graphene's Phase Transition in Polymer Matrices. *Nano Lett.* **2009**, *9*, 2129–2132.
14. Fasolino, A.; Los, J. H.; Katsnelson, M. I. Intrinsic Ripples in Graphene. *Nat. Mater.* **2007**, *6*, 858–861.
15. Katsnelson, M. I.; Geim, A. K. Electron Scattering on Microscopic Corrugations in Graphene. *Philos. Trans. R. Soc. A* **2008**, *366*, 195–204.
16. Ohta, T.; Bostwick, A.; Seyller, T.; Horn, K.; Rotenberg, E. Controlling the Electronic Structure of Bilayer Graphene. *Science* **2006**, *313*, 951–954.
17. Mariani, E.; von Oppen, F. Flexural Phonons in Free-Standing Graphene. *Phys. Rev. Lett.* **2008**, *100*, 076801-4.
18. Jia, X.; Hofmann, M.; Meunier, V.; Sumpter, B. G.; Campos-Delgado, J.; Romo-Herrera, J. M.; Son, H.; Hsieh, Y.-P.; Reina, A.; Kong, J.; Terrones, M.; Dresselhaus, M. S. Controlled Formation of Sharp Zigzag and Armchair Edges in Graphitic Nanoribbons. *Science* **2009**, *323*, 1701–1705.
19. Xu, Z.; Zheng, Q.-S.; Chen, G. Elementary Building Blocks of Graphene-Nanoribbon-Based Electronic Devices. *Appl. Phys. Lett.* **2007**, *90*, 223115-3.
20. Xu, Z. Graphene Nano-Ribbons under Tension. *J. Comput. Theor. Nanosci.* **2009**, *6*, 625–628.
21. Xu, Z.; Xue, K. Engineering Graphene by Oxidation: A First Principles Study. *Nanotechnology* **2010**, *21*, 045704-7.
22. Xue, K.; Xu, Z. Strain Effects on Basal-Plane Hydrogenation of Graphene: A First-Principles Study. *Appl. Phys. Lett.* **2010**, *96*, 063103-3.
23. Chaikin, P. M.; Lubensky, T. C. *Principles of Condensed Matter Physics*; Cambridge University Press: Cambridge, UK, 1995.
24. Chen, X.; Hutchinson, J. W. A Family of Herringbone Patterns in Thin Films. *Scripta Mater.* **2004**, *50*, 797–801.
25. Shenoy, V. B.; Reddy, C. D.; Ramasubramaniam, A.; Zhang, Y. W. Edge-Stress-Induced Warping of Graphene Sheets and Nanoribbons. *Phys. Rev. Lett.* **2008**, *101*, 245501-4.
26. Abraham, F. F.; Rudge, W. E.; Plischke, M. Molecular Dynamics of Tethered Membranes. *Phys. Rev. Lett.* **1989**, *62*, 1757–1760.
27. Wang, L.; Zheng, Q.; Liu, J. Z.; Jiang, Q. Size Dependence of the Thin-Shell Model for Carbon Nanotubes. *Phys. Rev. Lett.* **2005**, *95*, 105501-4.
28. Xu, Z.; Zheng, Q.-S.; Chen, G. Thermally Driven Large-Amplitude Fluctuations in Carbon-Nanotube-Based Devices: Molecular Dynamics Simulations. *Phys. Rev. B* **2007**, *75*, 195445-4.
29. Hedgeland, H.; Fouquet, P.; Jardine, A. P.; Alexandrowicz, G.; Allison, W.; Ellis, J. Measurement of Single-Molecule Frictional Dissipation in a Prototypical Nanoscale System. *Nat. Phys.* **2010**, *5*, 561–564.
30. Schnurr, B.; Gittes, F.; MacKintosh, F. C. Metastable Intermediates in the Condensation of Semiflexible Polymer. *Phys. Rev. E* **2002**, *65*, 061904-13.
31. Cranford, S.; Sen, D.; Buehler, M. J. Meso-Origami: Folding Multilayer Graphene Sheets. *Appl. Phys. Lett.* **2009**, *95*, 123121-3.
32. Martins, B. V. C.; Galvao, D. S. Curved Graphene Nanoribbons: Structure and Dynamics of Carbon Nanobelts. *Nanotechnology* **2010**, *21*, 075710-6.
33. Shi, X.; Pugno, N.; , M.; Cheng, Y.; Gao, H. Gigahertz Breathing Oscillators Based on Carbon Nanoscrolls. *Appl. Phys. Lett.* **2009**, *95*, 163113-3.
34. Li, Z.; Cheng, Z.; Wang, R.; Li, Q.; Fang, Y. Spontaneous Formation of Nanostructures in Graphene. *Nano Lett.* **2009**, *9*, 3599–3602.
35. Bao, W.; Miao, F.; Chen, Z.; Zhang, H.; Jang, W.; Dames, C.; Lau, C. N. Controlled Ripple Texturing of Suspended Graphene and Ultrathin Graphite Membranes. *Nat. Nano* **2009**, *4*, 562–566.
36. Plimpton, S. Fast Parallel Algorithms for Short-Range Molecular Dynamics. *J. Comput. Phys.* **1995**, *117*, 1–19.
37. Brenner, D. W.; Shenderova, O. A.; Harrison, J. A.; Stuart, S. J.; Ni, B.; Sinnott, S. B. A Second-Generation Reactive Empirical Bond Order (REBO) Potential Energy Expression for Hydrocarbons. *J. Phys.: Condens. Matter* **2002**, *14*, 783–802.